David Tomás Sánchez Martínez
Lourdes García Rodríguez
(coordinadores)

Proceedings of the 7th International Seminar on ORC Power Systems

Editorial Universidad de Sevilla

Proceedings of the 7th International Seminar on

ORC

Power Systems

David Tomás Sánchez Martínez
Lourdes García Rodríguez
(coordinadores)

Proceedings of the 7th International Seminar on

ORC Power Systems

(ORC2023)

4th to 6th
SEPTEMBER
SEVILLE 2023

EDITORIAL UNIVERSIDAD DE SEVILLA

Sevilla, 2024

Colección Actas
Núm.: 91

Review chairs of the 7th Internation Seminar on ORC Power Systems

Prof. Christoph Wieland (University of Duisburg-Essen) - *Review Chair*
Prof. Sotirios Karellas (National Technical University of Athens) - *Review Co-Chair*
Prof. Teemu Turunen-Saaresti (LUT University) - *Review Co-Chair*
Dr. Diego-César Alarcón-Padilla (Plataforma Solar de Almería - CIEMAT) - *Review Co-Chair*
Dr. Francesco Crespi (Universidad de Sevilla) - *Review Co-Chair*

ISBN 978-84-472-2745-7
DOI: https://dx.doi.org/10.12795/9788447227457

Diseño de cubierta y maquetación: los autores

INDEX OF CONTRIBUTIONS

DOI: https://dx.doi.org/10.12795/9788447227457_142
Paper ID #142, page 1 of 11

AERODYNAMIC DESIGN AND NUMERICAL ANALYSIS OF A COUNTER-ROTATING CENTRIFUGAL COMPRESSOR

Cheikh Brahim ABED*, Arthur LEROUX,

ENOGIA, 19 Av. Paul Héroult, Marseille, France

*Corresponding Author: cheikh-brahim.abed@enogia.com

ABSTRACT

Counter-rotating turbomachines offer more design and control options than conventional machines. While axial counter-rotating turbomachines have been widely studied, few studies have focused on centrifugal ones. This paper presents a detailed numerical study on the benefits of counter-rotating impellers for centrifugal compressors, specifically the impact of speed ratio on performance gain. The study used 0D/1D models and optimization methods to meet design criteria. The aerodynamic performance of the new designs was compared to a baseline configuration consisting of a centrifugal impeller and a vaned wedge diffuser. The new design features a first impeller with perfect axial inlet and mixed flow or a purely radial blade at the impeller exit, and a parametrically designed counter-rotating bladed diffuser with radial or mixed flow inlet and radial outlet. Optimized solutions were determined using validated 0D/1D loss models and analyzed using a 3D CFD solver. The results show that this new configuration can increase efficiency on a wide range compared to the baseline using speed ratio modulation.

1 INTRODUCTION

Counter-rotating CR turbomachines with two rotors were promising for improving performance, such as efficiency, power density, and operating range. However, previous studies have primarily focused on axial machines, which have shown that the most significant advantage of CR machines is the additional degree of freedom, namely the speed ratio ($\theta = N_{FR}/N_{RR}$) compared to single-rotor machines SR. In CR machine, the upstream or front rotor is named FR while the downstream or rear one is called RR and are rotating in opposite direction as shown in Fig.1. 761

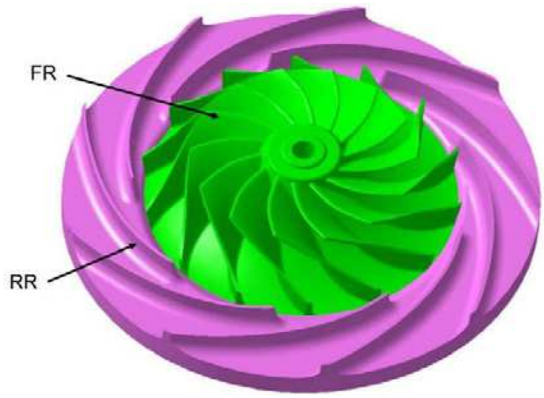

Figure 1: FR and RR rotors for a CR centrifugal compressor

A literature review on CR machines conducted in previous studies (Abed et al., 2020, 2021, 2022) revealed that, for axial CR configurations, adjusting the speed ratio θ of impellers in axial CR compressors enhances pressure rise and stall margin. When rear rotor RR rotating faster than front rotor FR, stall suppression is increased by almost 50%. Boosting the rotational speed of FR improves maximum efficiency, but marginally decreases pressure rise. Conversely, lowering the speed of FR while maintaining RR's speed results in fewer stable operating conditions. Furthermore, it was discovered that RR is more prone to stalling when the speed ratio exceeds 0.9, and its leakage flow

decreases at a lower speed than FR. Similarly, adjusting the speed ratio positively impacts the performance of counter-rotating axial pumps and fans.
Moreover, in radial counter-rotating CR configurations, the previous literature survey has demonstrated that the speed ratio θ plays a significant role in enhancing the overall performance of CR mixed-flow pump. This is attributed to the fact that by determining the optimal rotational speed for FR and RR at each operating point, the power density offered by the CR configuration can be maximized compared to the baseline single rotor SR. This optimization can be achieved by rotating RR at a higher speed than the FR for low flow rates and vice versa. Additionally, the literature survey reveals that blockage tends to occur earlier in CR machines compared to their SR counterparts. Similar observations regarding the impact of the speed ratio between FR and RR on the performance of CR mixed-flow pumps have been made in the context of CR radial fans. (Dejour and Vo, 2018) research on a hybrid configuration, which consists of a mixed-flow impeller as FR and an axial impeller as RR, reveals a substantial increase in pressure rise compared to a single rotor SR. However, this improvement does not coincide with a corresponding increase in efficiency. It is also noteworthy that blockage tends to occur earlier in this CR configuration compared to SR.
Furthermore, the work of (Abed et al., 2020, 2021, 2022) recently carried out extensive research to develop a validated design method for counter-rotating CR centrifugal compressor. This work was driven by the limited information found in the literature concerning the design approach and performance analysis of such machines. The cited studies on CR centrifugal compressor configurations primarily concentrate on the design method, its experimental and numerical validation, and a broad performance comparison with single rotor (SR) configurations. However, these investigations have not specifically explored the influence of the speed ratio on operating conditions and its wider implications, which is one of the main aims in the current work.
In this study, unshrouded impellers are employed for the CR configuration to facilitate comparison with the baseline single rotor SR. The SR configuration here consists of a single centrifugal impeller and a wedge-vaned diffuser, for which limited experimental and geometrical data can be found in Gaetani et al. (2012). The primary objective of this work is to emphasize the performance improvements offered by the CR configuration in comparison to the SR machine.

2 DESIGN METHOD

2.1 Velocity triangles

The key to design CR rotors is the correct formulation of its velocity triangles and understanding what implies. FR and SR rotors are similar and so are they're velocity triangles. However, RR is a counter-rotating rotor, so its inlet velocity triangles are distinctive because of its strong inlet counter swirl as shown by Fig. 2. Small gap of $J = 4mm$ is considered between FR and RR and to assume that no change occurs between FR and RR in terms flow properties of velocity triangles:

$$C_2 = C_3, C_{t2} = C_{t3}, C_{m2} = C_{m3} \tag{1}$$

The tangential component of absolute velocity at the outlet of FR, C_{t2}, contributes to increase the tangential component of the relative velocity at the inlet of RR impeller as:

$$W_{t3} = U_3 + C_{t3} \tag{2}$$

Eqn. 2 shows how the relative velocity at the inlet of RR increases by the counter-rotating effect.
This can lead to transonic or sonic inlet conditions and should be considered in the design procedure of CR. To compare the increase of enthalpy provided by CR and SR, RR outlet diameter is assumed equal to the peripheral diameter of SR impeller. Rotational speed of SR impeller and RR are also assumed to be equal, so we have $U_{2SR} = U_{4RR}$. Using the Euler's formula for ideal flow and assuming no pre-swirl at the inlet suction of both configurations, we can write the enthalpy rise of SR using Eqn.3:

$$\Delta h_{SR} = U_{2SR}.C_{t2SR} \tag{3}$$

The enthalpy rise of CR is the sum of each FR and RR enthalpy rise as expressed by Eqn. 4:

$$\Delta h_{CR} = \Delta h_{FR} + \Delta h_{RR} \tag{4}$$

RR rotational direction is considered as the positive one. The enthalpy rise of FR can be expressed using Eqn.5:

$$\Delta h_{FR} = (-U_2).(-C_{t2}) = U_2.C_{t2} \tag{5}$$

And the enthalpy of RR having negative pre-swirl at inlet can be formulated using Eqn. 6:

$$\Delta h_{RR} = U_4 . C_{t4} - (U_3).(-C_{t3}) = U_4 C_{t4} + U_3 C_{t3} \tag{6}$$

Assuming ideal flow and the same outlet blade angle for SR impeller and RR with $U_{2SR} = U_{4RR}$, the increase of enthalpy given by CR compared to SR is in fact $U_3 C_{t3} + U_2 C_{t2}$.

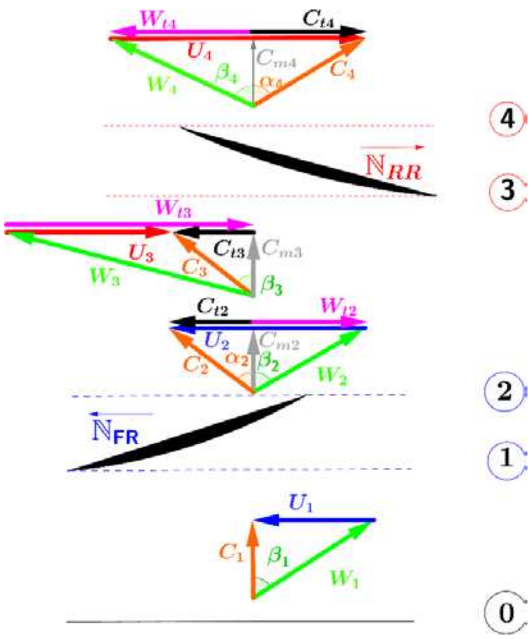

Figure 2: CR centrifugal compressor velocity triangles, (0): inlet station, (1): FR leading edge, (2): FR trailing edge, (3): RR leading edge, (4): RR trailing edge 763

2.2 CR Design approach

In the present work, two additional features have been added to a previous design procedure presented in (Abed et al., 2020, 2021) This approach for CR presented in Fig. 3 is composed of a 0D/1D design method coupled with NSGA-II optimization algorithm. The geometric parametrization of CR including FR and RR is summarized in Fig. 4.

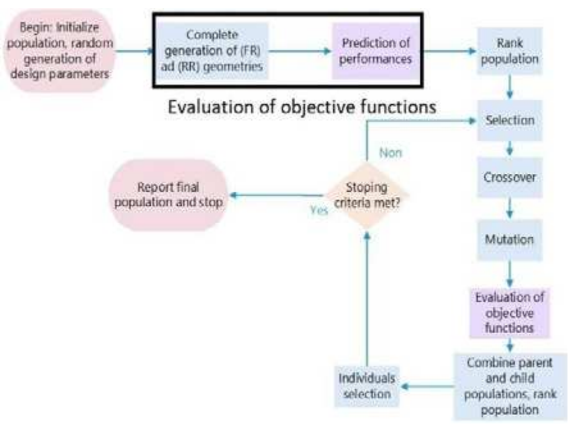

Figure 3: CR centrifugal compressor design flowchart

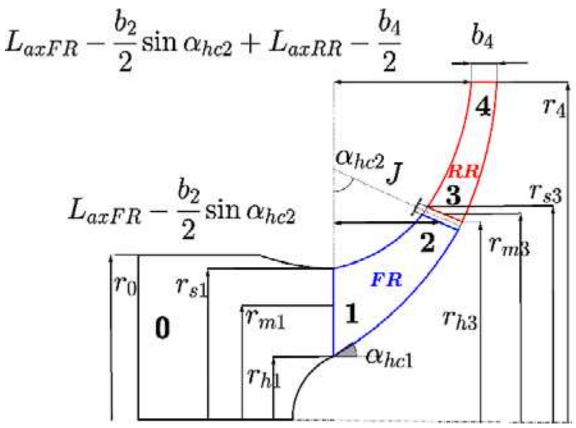

Figure 4: CR centrifugal compressor geometrical design parameters

It was found that the predicted outlet flow of FR is not quite accurate in some design operating conditions, so an additional step in the design of FR is considered by evaluating its performance using an adapted set of loss models developed in the thesis of (Abed 2021) and published in the paper

(Abed et al., 2021) in which an experimental validation of the design method is presented.

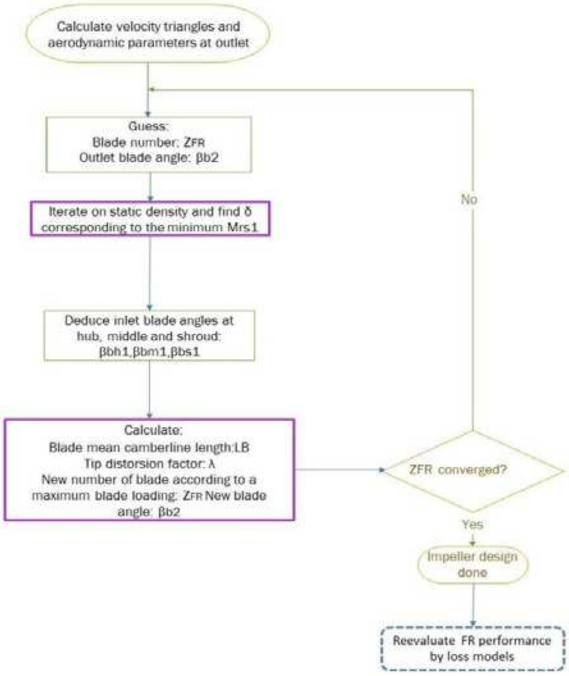

Figure 5: FR design flowchart, updated from (Abed,2020)

3 CASE STUDY

The case study in this paper is a design of CR configurations based on a baseline centrifugal compressor 764
SR selected from literature. The aim is to design a CR configuration having the same outlet diameter of RR as that of SR impeller.

3.1 Reconstruction of SR configuration based on available data

The baseline configuration SR considered in this study is a conventional high specific-speed centrifugal compressor composed of a radial impeller and a wedge vaned diffuser. Geometrical parameters and experimental measurements at three operating conditions in which the impeller rotates at 12.5 kRPM can be found in the work of Gaetani et al. (Gaetani et al. 2012) and summarized in Tabs. (1-2). Some important geometrical parameters of the baseline are not provided such as clearance gap and axial distance. To estimate those values, clearance gap was fixed at 5% of impeller blade width $b2$ and axial distance is calculated iteratively to match the desired pressure ratio of 1.6 of the whole stage. At every value of Lax, the complete geometry of SR impeller and the wedge vaned diffuser is generated, and then the pressure is estimated using the previous validated set of loss models. Fig. 11 shows the flowchart of axial distance calculation. The value obtained for the axial distance of the baseline SR is $L_{ax} = 114.2\ mm$. Figures 12 and 13 show respectively the blade angle distribution from inlet to outlet and the meridional view of the SR impeller. The wedge vaned diffuser is built in the same way as that of SR impeller considering a purely radial meridional variation and constant variation of the blade angle distribution. Figure 14 shows the comparison of total-total pressure ratio obtained from CFD calculations and experimental data. SM is the CFD simplified model using single passage per component and FM is the full model using all passages.

Table 1: SR main geometrical parameters extracted from (Gaetani et al. 2012)

Radial Impeller				
r_{s1}	r_{s1}	b_2	Z_{SR}	$\boldsymbol{\beta}_{b2}$
131,5 mm	200 mm	17.4 mm	16	-24°
Vanned wedge diffuser				
r_3	r_4	$b_3 = b_4$	Z_{dif}	$\boldsymbol{\beta}_{b2}$
220 mm	382.5 mm	22 mm	25	63°

Table 2: SR operating conditions, extracted from (Gaetani et al. 2012)

	Near stall	**Best efficiency**	**Near choke**
$\dot{m}$ [kg/s]	2.61	3.28	4.7
π_{t4}	1.56	1.605	1.48

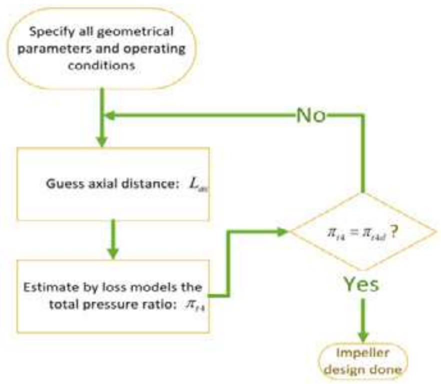

Figure 11: SR axial distance calculation of SR impeller

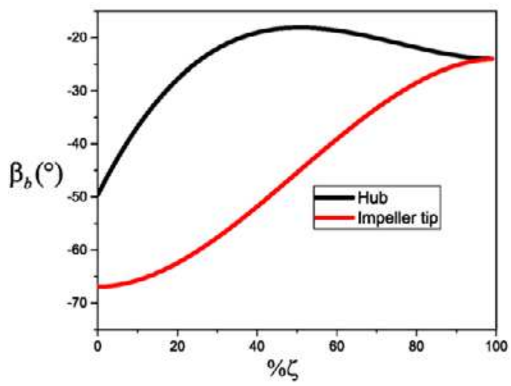

Figure 12: Blade angle distribution pf SR impeller

765

Tab. 4 resumes the errors between CFD calculations for the constructed SR configuration and experimental data of the baseline SR extracted from (Gaetani et al. 2012) at three operating conditions. These errors are small enough to be acceptable. Fig. 15 shows the original baseline and the reconstructed one by the developed tool.

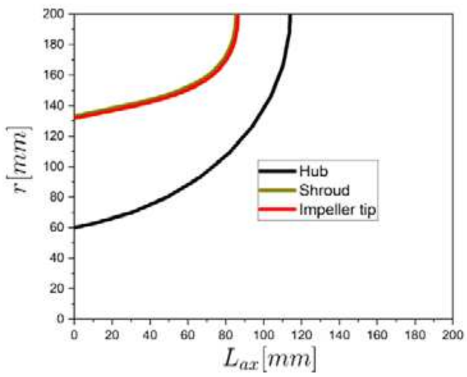

Figure 13: Meridional shape of SR impeller

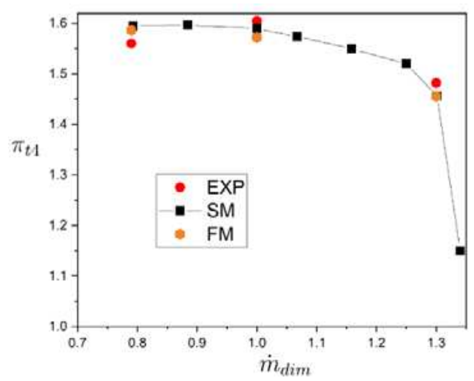

Figure 14: Pressure ration comparison between CFD and experimental of SR

Table 4: Validation of the constructed baseline SR

Pressure ratio	Experimental data	CFD (SM)	Error (%)	CFD (FM)	Error (%)
Near stall	1.56	1.595	2.24	1.585	1.6
Best efficiency	1.605	1.589	0.997	1.572	2.05
Near choke	1.482	1.456	1.754	1.455	1.78

Figure 15: Original SR (left) and constructed SR (right)

3.2 CR design method

The design of CR follows the method specified in [15]. The interface of FR and RR is determined by the factor $\chi_{FR} = r_2/r_4$ which defines indirectly the specific amount of enthalpy increase that FR and RR should give.

For the optimization loop, the set of parameters: $\chi_{FR}, b_5, \beta_{b5}, N_{FR}, N_{RR}$ presents the decision variables while some constraints have been specified such as the relative Mach number at the inlet of RR to avoid choke. The operating mass flow is fixed by the designer and corresponds here to the design mass flow of SR which correspond to the best operating point. Finally, the two objectives of optimization are the maximization of total-total pressure ratio π_{t4} and the corresponding isentropic efficiency η_{t4} of CR. Finally, the range of design parameters are described as following:

$$\dot{m}_d = 3.28 kg/s,$$

$$0.3 \leq \chi_{FR} \leq 0.77,$$

$$10\ kRPM \leq N_{FR} \leq 18\ kRPM,$$

$$10\ kRPM \leq N_{RR} \leq 12.5\ kRPM,$$

$$max(Mr_{thFR}, Mr_{thRR}) \leq 0.9,$$

$$0.1b_2 \leq b_5 \leq 3b_2, -90° \leq \beta_{b5} \leq 0°$$

The optimization procedure in the phase of CR design is presented in Fig. 3. In this flowchart, the step framed in black color corresponds to the evaluation of the objective functions according to NSGA-II algorithm in which the design and performances of FR and RR are performed by the in-house code.

4 RESULTS

4.1 Optimization results

The Pareto front obtained from optimization for CR configuration is shown in Fig 16. Pareto front shows a large variation of π_{t4} from 1.84 to 2.4 according to a slight variation η_{t4}. χ_{FR}. The Pareto front obtained from optimization for CR configuration is shown in Fig 16. Pareto front shows a large variation of π_{t4} from 1.84 to 2.4 according to a slight variation η_{t4}. χ_{FR}varies between 0.51 to 0.78 is while the value of N_{RR} remains between $11.35kRPM$ to $12.49kRPM$. The value of N_{FR} is between $16.85\ kRPM$ to $17.89\ kRPM$. 11 prototypes are selected from Pareto front to be analyzed using 3D CFD simulations.

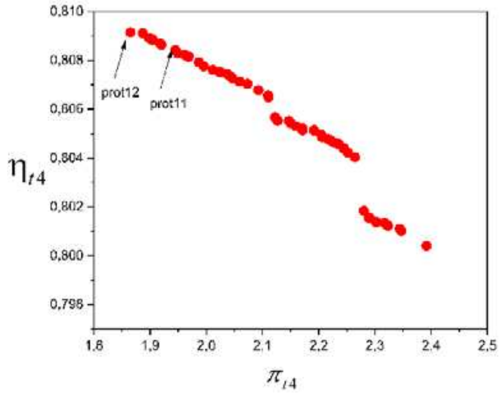

Figure 16: Pareto front obtained from the design optimization of CR configurations

4.2 Numerical method

The numerical calculations were carried out using a commercial CFD software ANSYS 2022R2. Simulations were performed using high resolution for advection scheme and turbulence equations. The $k-\omega$ SST turbulence model is employed. Calculations with mixing-plane interface are carried out to obtain the performance of all CR configurations with SR. For the sake of time and computational cost, a simplified passage model SM with rotational periodicity for component is simulated to generate the performance. Full model simulations are carried out also to assess the SM model. The fluid domain using air ideal gas contains an inlet pipe, two impellers and a vaneless diffuser for CR configurations and one impeller along with a vaned diffuser for SR. Fig. 17 shows the details of computational mesh for SR and a CR configuration. Theses meshes are obtained after a mesh sensitivity study with values about 2.45 millions elements for CR and 3.25 millions elements for SR. 767

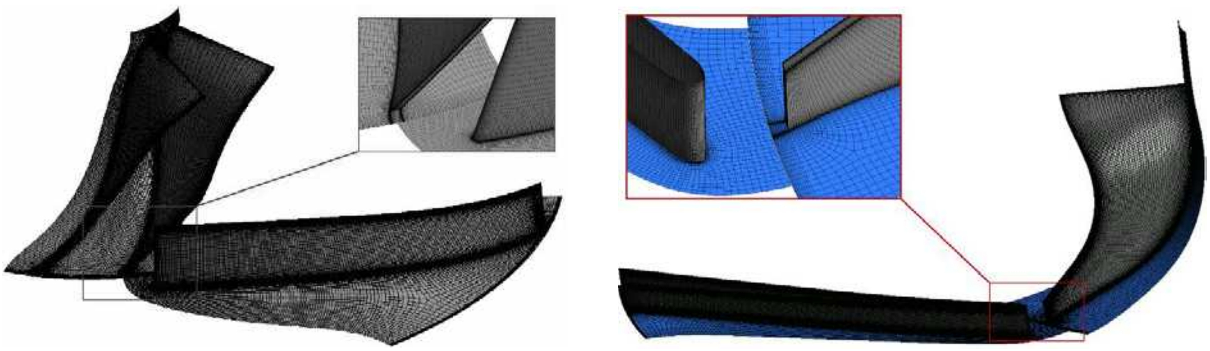

Figure 17: Blade mesh details of CR (left) and SR (right)

4.3 Obtained results

Fig. (18-19) show the performances of 11 simulated configurations of CR (prot1 to prot11) as well as SR. The total-total pressure ratio and the corresponding isentropic efficiency are calculated as:

$$\pi_{t4} = \frac{p_{t4}}{p_{t0}}, \qquad \eta_{t4} = \frac{\dot{m}.C_p.T_{t0}\left(\pi_{t4}^{\frac{\gamma-1}{\gamma}} - 1\right)}{\Gamma_{FR}.\omega_{FR} + \Gamma_{RR}.\omega_{RR}} \tag{12}$$

All parameters are calculated using area-averaged based on a section located at $r = 1.18\, r_{TE}$.

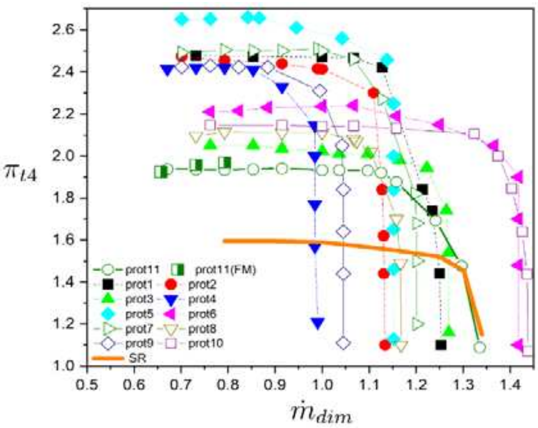

Figure 18: Total-total pressure ratio of 11 CR compressors selected from Pareto front

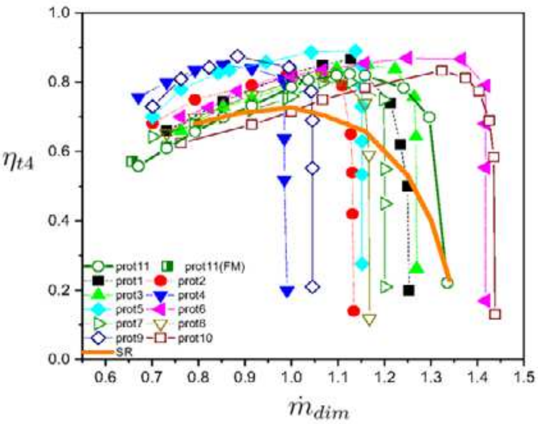

Figure 19: Isentropic efficiency of 11 CR compressors selected from Pareto front

The full model (FM) is also used on prot11 to assess the simplified model with one passage per component at low mass flow and both results are in good agreement. From these figures, one can see that prot10 and prot6 give the largest choking margin with a large efficiency. Prot4 gives the lowest choking margin and prot5 gives the highest pressure rise of the selected CR configurations. prot11 gives the lowest pressure rise, an acceptable choking margin and the largest stall margin. It has the lowest value of $\text{chi}_{\{FR\}} = 0.51$. Fig. 20 shows a clear comparison between the prot11 and SR. The static pressure is illustrated at the Hub surfaces, while turbulent kinetic energy (TKE) is shown on the blade surfaces. As mentioned before, since the outlet diameter and the rotation speed are identical for prot11 and SR, a fear comparison of the pressure rise between them can be illustrated. Higher static pressure is reached by the prot11 at the outlet. However, the TKE is also higher on the blade surfaces of RR than that of SR because of the high interactions between the FR and RR impellers. All CR configurations deliver higher efficiency and pressure ratio compared to the baseline SR. The total-total and total-static pressure rise coefficients are calculated using Eqn. 14.

$$\Psi_4 = \frac{p_4 - p_{t0}}{0.5\rho_{t0}{U_4}^2}, \Psi_{t4} = \frac{p_{t4} - p_{t0}}{0.5\rho_{t0}{U_4}^2} \qquad (13)$$

4.4 Effect of the speed ratio on the performance of CR machine: Case of prot12

Prot12 gives the lowest pressure ratio of all selected CR configurations and therefore selected to be further analyzed in terms of pressure rise and efficiency by speed ratio θ modulation while RR rotational speed remains fixed $N_{RR} = 12.5kRPM$.

Fig. 21 shows the evolution of total-total pressure rise and the corresponding isentropic efficiency coefficient according to a variation of θ in which the choke and stall margin are improved drastically. At design conditions $\dot{m}_{dim} = \dot{m}/\dot{m}_d = 1.0$, $\theta = 1.44$, $N_{RR} = 12.5kRPM$, prot12 delivers an increase of pressure rise about 87% and efficiency about 12% compared to SR.

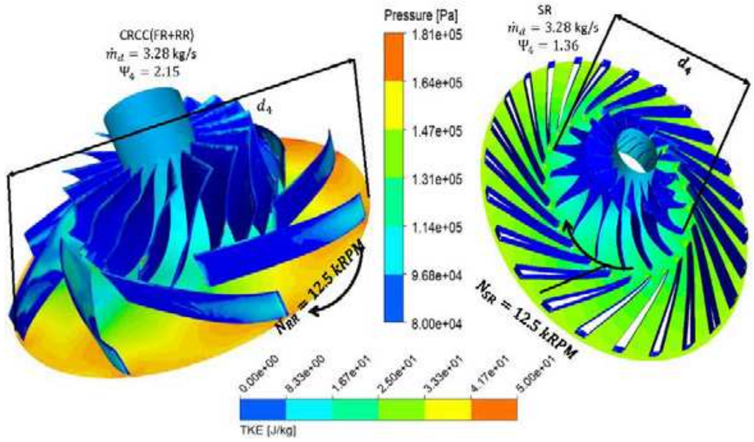

Figure 20: Comparison between the prot11 (left): design mass flow $\dot{m}_d = 3.28kg/s$ and corresponding pressure rise coefficient $\Psi_{t4} = 2.1$, RR speed $\omega_{RR} = 208.3\ Hz$ and conventional SR (impeller and vaned diffuser), (right): $\dot{m}_d = 3.28kg/s$ for pressure rise coefficient of $\Psi_{t4} = 1.4$, $\omega_{SR} = 208.3\ Hz$.

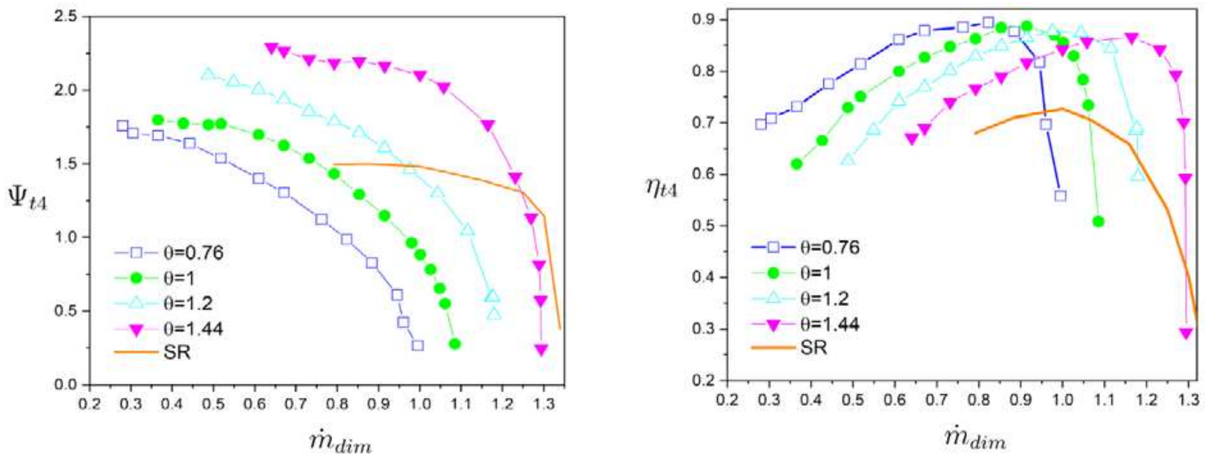

Figure 21: total-total pressure rise coefficient evolution (left) and corresponding isentropic efficiency (right) according to a variation of θ while $N_{RR} = 12.5kRPM$

769

Another advantage of the CR configuration is the increase of power density by a factor of 5 compared to SR as shown in Fig. 22 at design condition. The isentropic power density is defined as the power to the size of the machine and calculated by Eqn. 14. SR configuration was designed to produce a total-total pressure ratio of 1.6. By using the CFD data of prot12, it is possible to obtain a maximum totat-total isentropic efficiency for a fixed value of total-total pressure ratio of 1.6 by changing the peripheral speed of both FR and RR impellers as shown in Fig. 23. This figure shows that the nondimensional efficiency area of prot12 is 2.88 times higher than that of SR. This parameter is calculated using Eqn. 15.

$$Power_t = \frac{\dot{m} C_p T_{t0} \left((p_{t4}/p_{t0})^{\frac{\gamma - 1}{\gamma}} - 1 \right)}{\pi {r_4}^2 L_{ax} \rho_{t0}} \tag{14}$$

$$S = \int_{\dot{m}_{stall}}^{\dot{m}_{choke}} \frac{\eta_{t4}}{\dot{m}_d} d\dot{m} \tag{15}$$

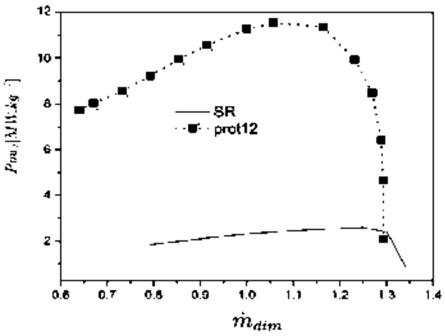

Figure 22: Isentropic power density comparison of prot12 and SR

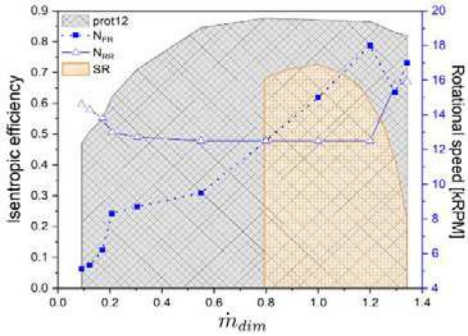

Figure 22: Area of Isentropic power density comparison of prot12 and SR

5 CONCLUSIONS

The objective of this work is to present a detailed design optimization method applied to CR configurations in centrifugal compressor stages and to highlight their advantage compared to standard configuration SR focusing on the effect of speed ratio of CR and its effect on the performance. Thereby, a Meanline approach coupled with optimization techniques is proposed allowing an efficient design of CR. During the design step and because of the compressibility of the flow, specific attention is considered when designing the inlet of RR to obtain an acceptable blockage margin. Furthermore, 12 configurations selected from Pareto front are analyzed by using a 3D CFD solver. The obtained results illustrate global performance improvement with respect to the same outlet radius and peripheral speed of the baseline. By modulating the speed ratio of FR and RR, it's possible to improve the stall and choke margin while increasing the efficiency on a wide range of operating points. The results show that the isentropic total-total power density is increased by a factor of 5 compared to that of SR.

Nomenclature

N, ω	Rotational speed	(RPM, rad/s)
θ	Speed radio (-)	
C	Absolute velocity	(m/s)
W	Relative velocity	(m/s)
U	Peripheral speed	(m/s)
Δh	Enthalpy rise	(J/kg)
b	Blade width	(m)
τ	Boundary layer thickness	(m)
T	Temperature	(K)
p	Pressure	(Pa)
β_b	Blade angle	(°)
ρ	Density	(kg.m^{-3})
π	Pressure ratio(-)	
η	Isentropic efficiency	
Γ	Torque	(N.m)

Subscript

FR	Front impeller

RR Rear impeller
t Total condition, tangentiel component
m Meridional composent
CR Counter-rotating configuration
SR Baseline
th Throat conditions

REFERENCES

Abed, C.B., Khelladi, S., Deligant, M., El Marjani, Bakir, F., 2020, Preliminary Study of a Centrifugal Compressor With Counter-Rotating Impellers: Design and Performances Study. *Turbo Expo: Power for Land, Sea, and Air. Vol. 84102. American Society of Mechanical Engineers.*

Bourabia, L., Abed, C. B., Cerdoun, M., Khalfallah, S., Deligant, M., Khelladi, S., & Chettibi, T., 2021. Aerodynamic preliminary design optimization of a centrifugal compressor turbocharger based on one-dimensional mean-line model. Engineering Computations, 38(9), 3438-3469.

Abed, C. B., Khelladi, S., Deligant, M., El Marjani, A., Solis, M., & Bakir, F. 2021. Experimental Validation of the Aerodynamic Performance of an Innovative Counter-Rotating Centrifugal Compressor. Energies, 14(9), 2582.

Nguyen, V. T., Abed, C. B., Danlos, A., Ravelet, F., Paridaens, R., Deligant, M., Bakir, F. 2022. Experimental study of a novel centrifugal compressor with two successive and independent rotors. *J. of Engineering for Gas Turbines and Power, 144(1).*

Dejour, Q., Vo, H. D., 2018, Assessment of a novel non-axial counter-rotating compressor concept for aero-engines. *In Turbo Expo: Power for Land, Sea, and Air (Vol. 50992, p. V02AT39A041). American Society of Mechanical Engineers.*

Aungier, R.H., 2000, Centrifugal compressors: A strategy for aerodynamic design and analysis. *American Society of Mechanical Engineers Press: New York, NY, USA.*

Abed, C.B., 2021, Modélisation, Analyse et Contrôle des Compresseurs Centrifuges Contrarotatifs: *Aérodynamique Numérique et Expérimentale, Ph.D Thesis, Arts et Métiers Institute of Technology, ParisTech, France.*

Japikse, D., 1986, Advanced topics in turbomachinery technology, Concepts Eti.

Oh, H. W., Yoon, E. S., & Chung, M. K., 1997, An optimum set of loss models for performance prediction of centrifugal compressors. *Proceedings of the Institution of Mechanical Engineers, Part A: J. of Power and Energy, 211(4), 331-338.*

McKain, T. F., Holbrook, G. J., 1997, Coordinates for a high performance 4: 1 pressure ratio centrifugal compressor, *No. E-10833, NTRS.*

Dolan, F. X., Runstadler Jr, P. W., 1979, Design, development, and test of a laser velocimeter for a small 8: 1 pressure ratio centrifugal compressor, *No. NASA-CR-134781, NTRS.*

Gaetani, P., Persico, G., Mora, A., Dossena, V., and Osnaghi, C., 2012, Impeller-Vaned Diffuser Interaction in a Centrifugal Compressor at Off Design Conditions. ASME. J. Turbomach. November 2012; 134(6): 061034.

This book contains the compilation of works contributed to the *7th International Seminar on Organic Rankine Cycle Power Systems* (ORC 2023), held in Seville between the 4th and 6th of September 2023. The event was hosted by Universidad de Sevilla on behalf of the Knowledge Centre on Organic Rankine Cycle Technology (KCORC), incorporated in The Netherlands.

The ORC conference, organized biennially, stems as the only conference that is specific to ORC technology, therefore gathering a diverse community whose affiliation spans across all the interested stakeholders, not only in this particular technology but also and in a broader context, in the energy transition. Original equipment manufacturers, professional associations, end-users, investors, policy makers, academics, scientists feel at home at ORC 2023.

The almost 100 proceedings in this book cover a wide variety of topics, from fundamentals to system integration through component design, accounting for thermodynamic performance as well as component design. In addition to this, and as a new track in 2023, works on heat pump technology were also accepted in order to raise awareness of the strong ties between both technologies, specifically in energy storage applications.

This book provides an excellent overview of the current maturity of power systems based on Organic Rankine Cycle technology for applications as diverse as geothermal and waste heat recovery in industry or downstream of other prime movers (e.g., marine applications). It is also an excellent source of information to understand the current challenges faced by the technology, stemming from a very competitive market and increasingly stringent environmental regulations.

The organizers of ORC 2023 hope that the reader finds this work as exciting as the attendees to the conference and, maybe, make the decision to join the 8th edition to the conference in 2025.

KCORC
KNOWLEDGE CENTER
ORGANIC RANKINE CYCLE

eus EDITORIAL
UNIVERSIDAD DE SEVILLA